# Analysis of EMI Terminal Modeling of Switched Power Converters

Hemant Bishnoi, *Student Member, IEEE*, Andrew Carson Baisden, *Member, IEEE*, Paolo Mattavelli, *Senior Member, IEEE*, and Dushan Boroyevich, *Fellow, IEEE*

***Abstract*—A generalized terminal modeling technique was proposed earlier to predict conducted electromagnetic interference from a dc–dc boost converter. The predictions of these conducted emissions showed that there was a good agreement up to 50 MHz. This paper extends the generalized terminal modeling approach to converters with the buck-type input. Both dc and ac applications are discussed. The technique is developed for the electromagnetic interference modeling of switched power converters in aerospace applications where the requirements on electromagnetic pollution are very strict. The model is shown to successfully predict conducted emissions for a buck converter and a three-phase voltage source inverter up to 100 MHz with an error of 6 dB or less at most frequencies.**

***Index Terms*—Buck converter, conducted emissions, EMI terminal modeling, Norton equivalents, voltage source inverter (VSI).**

## I. Introduction

SWITCHED power supplies are being widely used in both industrial and military applications. This class of power supplies has both high efficiency and reliability. However, they are also known to produce high levels of conducted electromagnetic interference (EMI) due to the fast voltage switching action ($dv/dt$) produced by the semiconductor switches. Thus, EMI filters are necessary to suppress the noise generated by switched power supplies.

Designing EMI filters for aerospace applications can be quite challenging as they need to be optimized for both weight and volume [1], [2]. Simple and accurate EMI models of power supplies are thus needed to facilitate the development of high-performance EMI filters. Typically, some forms of lumped circuit models are used for modeling EMI. A detailed lumped circuit model may consist of physics-based models of semiconductor devices and all the relevant parasitics in the circuit. In the case of power converters, such models often become too complex and produce convergence issues with the simulators. Thus, design and optimization of the EMI filter has been an art that mostly relied on trial-and-error methods. In fact, with the present state-of-the-art in EMI modeling of power supplies, it is difficult to predict conducted emissions beyond 10 MHz [3], [4]. Earlier attempts have also used trapezoidal waveforms to approximate the noise sources and simplified lumped circuit equivalents to model EMI [5]–[9]. These approximations usually lead to oversimplification at higher frequencies and hence seldom give accurate predictions above a few megahertz. In order to overcome the limitations of lumped circuit models, an alternative modeling style, broadly classified as behavioral modeling techniques, has been shown to achieve faster and more accurate predictions of EMI.

One of the earliest attempts in behavioral modeling [10] showed a resonance method for the extraction of input impedance of the power supply. However, the method is difficult to apply at frequencies where noise impedance may have several closely spaced resonances. In [11], a two-terminal Thevenin equivalent was used to model the common mode (CM) and differential mode (DM) noises separately for a three-phase inverter. The method, however, did not involve any mathematical de-embedding of the network connected to the terminals of the inverter. Thus, there may be inaccuracies in estimations of open-circuit noise voltage, which is required as per the definition of Thevenin theorem. In [12] and [13], a two-terminal Thevenin model was used for modeling CM and DM noises separately for a switched mode power supply. In [13], it was shown that the two-terminal models are having serious limitations in high frequency because of the mixed mode noise [14], [15].

In [16], a three-terminal Thevenin Equivalent was used to model electronic appliances. However, a vectored network analyzer (VNA) was used here to estimate the input impedances. Due to the limited power rating of the VNA, this method may not be easily applied to high-power converters. In [17], the same Thevenin model was used to model a buck converter but without using a VNA. In [18], a three-terminal model based on the Thevenin equivalents was used to model an isolated off-line half-bridge ac–dc converter. The system had been isolated from ground while modeling the DM portion of the three-terminal model, which could lead to inaccuracy since DM may not be completely decoupled from CM at higher frequencies [14], [15].

In [19] and [20], a three-terminal Norton equivalent was used to model a phase leg. However the model was only validated in a condition very close to one used for its extraction. The model uses only two impedances instead of three to represent a three-terminal Norton equivalent [21], thus limiting its accuracy. In [22]–[24], an improved three-terminal Norton equivalent was used to model a boost converter. The same model was

Manuscript received November 21, 2011; revised February 6, 2012; accepted February 14, 2012. Date of current version May 15, 2012. Recommended for publication by Associate Editor P. Tenti.

H. Bishnoi, P. Mattavelli, and D. Boroyevich are with the Department of Electrical and Computer Engineering, Virginia Tech., Blacksburg, VA 24060 USA (e-mail: hbishnoi@vt.edu; pmatta@vt.edu; dushan@vt.edu).

A. C. Baisden was with the Department of Electrical and Computer Engineering, Virginia Tech., Blacksburg, VA 24060 USA. He is now with the Johns Hopkins University Applied Physics Laboratory, Laurel, MD 20723 USA (e-mail: cbaisden@vt.edu).

Color versions of one or more of the figures in this paper are available online at http://ieeexplore.ieee.org.

Digital Object Identifier 10.1109/TPEL.2012.2190100

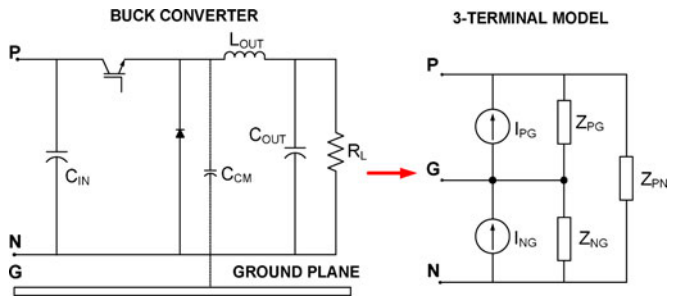


Fig. 1. Generalized three-terminal model of buck converter based on Norton equivalent.

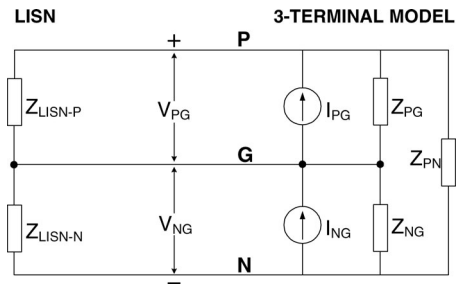


Fig. 2. Nominal case for model extraction.

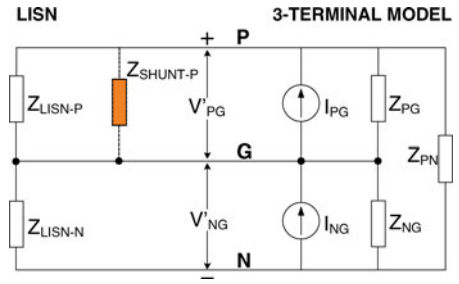


Fig. 3. Attenuated case for model extraction.

also reported in [24] but with a different extraction approach. In [25], the three-terminal Norton equivalent was applied to a buck converter and in [26] to a half-bridge inverter. Behavioral modeling was attempted in time domain as well [27], [28], and some works are devoted to only CM noise modeling [29], [30]. There are other works that address only noise impedance estimation [31]–[37].

Although these papers have shown successful application of two- or three-terminal models, they usually gloss over the fundamental reason that allows application of linear time-invariant (LTI) models to power converters. The true nature of these models and the limitations of such techniques have not been properly discussed before. This paper addresses the intricacies of EMI terminal modeling techniques. Limitations of the method and advantages that various postprocessing steps may offer are also discussed.

This paper is organized as follows. Section II describes the basic terminal modeling procedure. Sections III and IV show the experimental setup and modeling results for a buck converter, respectively. Section III also covers essential discussion on the applicability of terminal modeling method. Section V discusses the model errors and Section VI gives the validation results. Section VII extends the modeling technique to a three-phase inverter. Finally, Section VIII concludes this paper.

## II. Terminal Modeling Procedure

### A. Three-Terminal Model

This section reviews the generalized terminal modeling procedure. Fig. 1 shows a buck converter and its equivalent three-terminal EMI model. $C_{\rm CM}$ denotes the parasitic capacitance of the converter to the ground. The model has two current sources and three equivalent impedances. This model is a generic three-terminal Norton equivalent of a linear network. In Fig. 1, terminals positive (P), negative (N), and ground (G) are matched to the input terminals of the buck converter. The goal is to model the entire buck converter at these input terminals using the three-terminal model.

In the measurements of conducted emissions, it is required to isolate the device under test from the power source with a line impedance stabilization network (LISN). For modeling purposes, the LISN is replaced with its output impedances ($Z_{\rm LISN-P}$ and $Z_{\rm LISN-N}$), as shown in Fig. 2. The modeling procedure assumes that the converter appears to be linear and time invariant at its input terminals. This assumption, however, should be verified for every converter before terminal EMI modeling in carried out. The following loop equations can be derived from Fig. 2:

$$V_{\rm PG} = \left(I_{\rm PG} - \frac{V_{\rm PG} - V_{\rm NG}}{Z_{\rm PN}}\right) \cdot Z_{\rm PG} || Z_{\rm LISN-P} \tag{1}$$

$$V_{\rm NG} = \left(-I_{\rm NG} + \frac{V_{\rm PG} - V_{\rm NG}}{Z_{\rm PN}}\right) \cdot Z_{\rm NG} || Z_{\rm LISN-N}. \tag{2}$$

The case shown in Fig. 2 is referred to as the nominal case. In order to solve for five model parameters, other equations can be developed by adding shunt impedance(s) between P and G, between N and G, or both. These configurations are referred to as attenuated cases. Fig. 3 shows the attenuated case when the shunt impedance is applied to the positive side of the LISN. Equations (3) and (4) are derived from Fig. 3. Similarly, (5) and (6) are derived for the case when the shunt impedance is applied on the negative side of the LISN. Note that when the shunt is applied, the EMI noise voltages at the LISN change. Thus, voltage terms in all of the following equations are different for each case:

$$V'_{\rm PG} = \left(I_{\rm PG} - \frac{V'_{\rm PG} - V'_{\rm NG}}{Z_{\rm PN}}\right) \cdot Z_{\rm PG} || Z_{\rm LISN-P} || Z_{\rm SHUNT-P} \tag{3}$$

$$V'_{\rm NG} = \left(-I_{\rm NG} + \frac{V'_{\rm PG} - V'_{\rm NG}}{Z_{\rm PN}}\right) \cdot Z_{\rm NG} || Z_{\rm LISN-N} \tag{4}$$

$$V''_{\rm PG} = \left(I_{\rm PG} - \frac{V''_{\rm PG} - V''_{\rm NG}}{Z_{\rm PN}}\right) \cdot Z_{\rm PG} || Z_{\rm LISN-P} \tag{5}$$

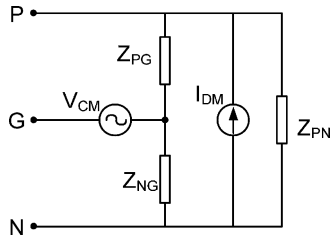


Fig. 4. Generalized three-terminal model with voltage and current sources.

$$V''_{\mathrm{NG}} = \left(-I_{\mathrm{NG}} + \frac{V''_{\mathrm{PG}} - V''_{\mathrm{NG}}}{Z_{\mathrm{PN}}}\right) \cdot Z_{\mathrm{NG}} || Z_{\mathrm{LISN-N}} || Z_{\mathrm{SHUNT-N}}. \tag{6}$$

Equations (1)–(4) and (6) can now be solved for $I_{\mathrm{PG}}$, $I_{\mathrm{NG}}$, $Z_{\mathrm{PG}}$, $Z_{\mathrm{NG}}$, and $Z_{\mathrm{PN}}$. The final closed-form solutions are complicated; hence, they are not shown here for the sake of simplicity [38]. This procedure, although shown here for a buck converter, in general is the same for any power converter with three terminals at its input. It should be noted that the model is always extracted at one operating point and hence cannot be used over a wide range of operating conditions. However, since the model is develop only for EMI, separate models for one or a few worst case operating conditions should be enough to address all EMI issues.

The model shown in Fig. 1 is just one of the possible topologies that can be used for system identification at EMI frequencies. As mentioned before, a Thevenin model can also be used. In fact, a mixed current and voltage source model such as the one shown in Fig. 4 is also possible. Here, $V_{\mathrm{CM}}$ represents the CM voltage with respect to ground and the current source $I_{\mathrm{DM}}$ is the DM currents drawn by the power supply. It should be noted that the model is extracted in an in-circuit test according to EMI standards, and therefore, the mixed mode noise effect is captured automatically in the two sources. In other words, the noise sources shown in Fig. 4 do not represent pure CM or pure DM noise. Though various topologies are possible, there was no significant difference seen in their accuracy. Therefore, in the rest of the paper, we use the model given in Fig. 1.

## III. Experimental Setup

### A. Buck Converter

The experimental setup is shown in Fig. 5. The buck converter operates as a dc–dc converter with 200 V dc input, and 100 V dc output across a 50 Ω load. The switching frequency $f_S$ is 100 kHz. The input capacitor $C_{\mathrm{IN}}$ is a 47 $\mu$F electrolytic capacitor. The diode is a 600 V/10 A silicon carbide (SiC) diode (C3D10060 A) from CREE and the insulated gate bipolar transistor (IGBT) (HGTG12N60A4) is a 600 V/12 A N-channel IGBT from Fairchild.

To attain better accuracy at high frequencies, the output impedances of the LISN ($Z_{\mathrm{LISN-P}}$ and $Z_{\mathrm{LISN-N}}$) and the shunt impedances ($Z_{\mathrm{SHUNT-P}}$ and $Z_{\mathrm{SHUNT-N}}$) were characterized with an Agilent 4294A impedance analyzer. The scope was set to capture one switching cycle of the converter. It is assumed

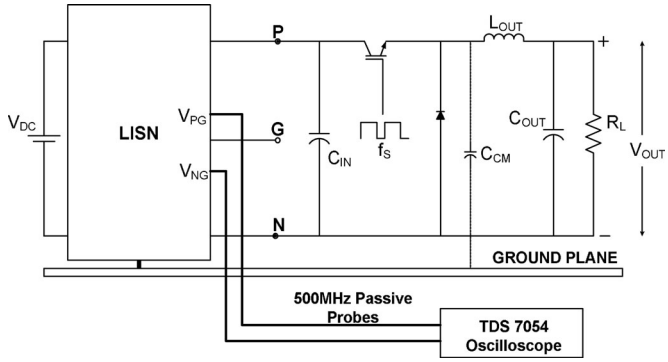


Fig. 5. Experimental setup for extraction of the three-terminal model of a buck converter.

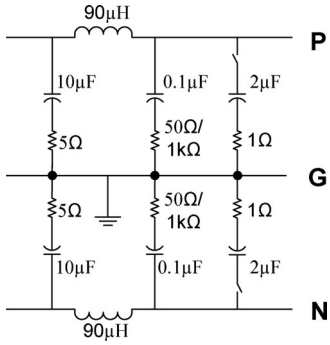


Fig. 6. Line impedance stabilization network (LISN).

that all switching cycles are fairly identical unless there is any change in the operating point of the converter. Averaging was used to remove the random noise and the data were recorded with a sampling time of 200 ps/point.

### B. Selection of External Network Impedance

The LISN used for experiments was modified to validate the terminal model under different source impedance conditions. A linear model should be independent of the external network in the desired frequency range and operating conditions. Thus, in order to validate the developed models, two different LISN impedances; 50 Ω and 1 kΩ, were chosen. The modified LISN is shown in Fig. 6. Selection switches were added to switch between 50 Ω and 1 kΩ output impedances. A well-conditioned model should be able to predict terminal voltages ($V_{\mathrm{PG}}$ and $V_{\mathrm{NG}}$) for both the 50 Ω and 1 kΩ LISNs [38].

An option for including the shunt impedances was also built into the LISN itself. This was done to minimize the effects of parasitics and obtain reproducible results. The shunt impedance used here is a series combination of a 2 $\mu$F capacitor and a 1 Ω resistor.

### C. Applicability of the Method

The terminal modeling method uses LTI circuits for approximating the EMI behavior of power converters. It is worthwhile to understand the conditions that allow the use of LTI theory for modeling a power converter which by nature is a nonlinear

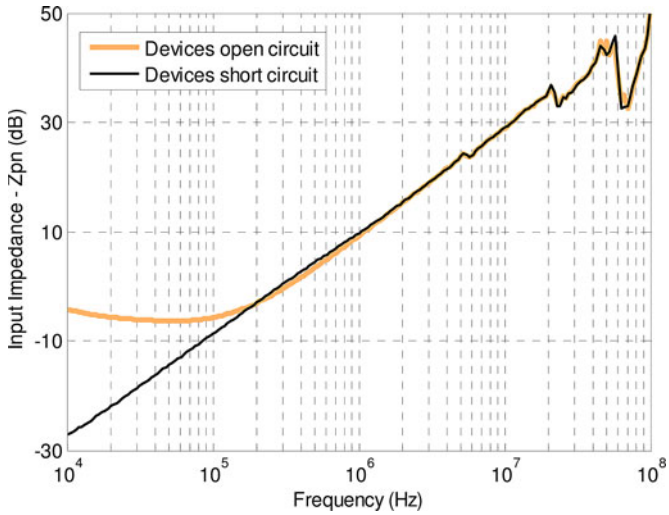


Fig. 7. Comparison of input DM impedance with the devices open and short circuited.

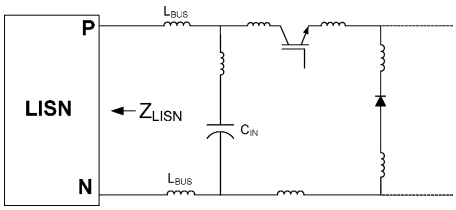


Fig. 8. Location of parasitic inductances in the input side of a buck converter.

and time-variant network. The discussions here are based on the buck converter described earlier in the experimental setup, but they should apply to any converter that has a buck type input.

The issue of time variance can be understood by considering the variation in the input impedance of the buck converter while it is in operation. Fig. 7 shows measurements of the DM impedance with an impedance analyzer (Agilent 4294A) for two extreme cases and an under zero dc bias condition (see Fig. 5). In the first measurement, the devices were physically removed, and in the second measurement the devices were short circuited. For a buck converter, these conditions will normally not exist but are chosen here only to show the worst case situations under all operating conditions. It can be seen from Fig. 7 that there is no significant difference in the input impedance in the conducted emissions range (150 kHz to 30 MHz) and even up to 100 MHz. At lower frequencies, some difference is seen; however, the impedance here is very small. The measurements show that the LISN does not see any significant change in the input impedance of the buck converter under all operating conditions, even during the time when the commutation takes place. The impedance seen in Fig. 7 is inductive after 100 kHz and comes from the parasitic inductances of the input dc bus ($L_{\mathrm{BUS}}$), as shown in Fig. 8. These parasitic inductances provide constant and dominant impedance that masks the time-varying behavior of the switches. Thus, looking from the dc-input side, the buck converted used here can be approximated as a time-invariant network. In a similar way, the CM input impedance can be shown to be constant as well.

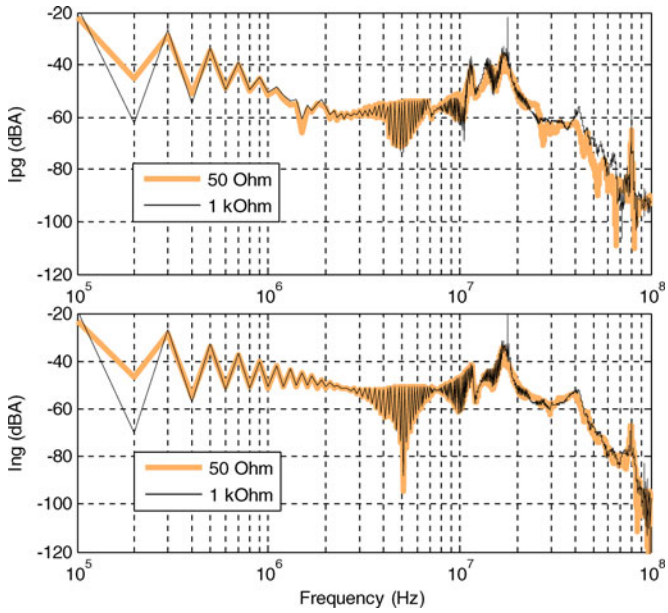


Fig. 9. Extracted noise sources $I_{\mathrm{PG}}$ and $I_{\mathrm{NG}}$ of the three-terminal model.

The three-terminal model uses two constant and linear current sources to capture the switching noise from the converter. In the case of a buck converter, such an approximation is possible with the presence of an input capacitor $C_{\mathrm{IN}}$. A properly chosen value of $C_{\mathrm{IN}}$ will ensure that the switching waveforms (voltage across the device and the current through the device) remain largely unaffected by any changes in the impedance that converters see into the dc network (LISN). The input capacitor must provide effective decoupling between the dc bus. The idea is to keep the impedance of the capacitive branch lower than the impedance of the dc bus ($Z_{\mathrm{LISN}} + Z_{\mathrm{Lbus}}$) in the entire frequency range to ensure that the switching energy is derived from the capacitor and not the dc source.

The basic inference from the previous discussion is that as long as the switching waveforms remain preserved from changes in the external network (LISN) and the converter appears time invariant at its input terminals, the terminal modeling method can be applied for approximating the EMI behavior of the power converter. The results shown here cannot be assumed for all power converters, especially the low power ones. Depending on the size and geometry of the converter, one should verify if these conditions hold or not. For most medium-to-high-power applications, these conditions are likely to hold true.

## IV. Modeling Results

A three-terminal model was developed for each LISN impedance (50 Ω and 1 kΩ) using the procedure described in Section II. It is worth noting that the models of an arbitrary three-terminal LTI circuit created from 50 Ω and 1 kΩ LISNs will be identical to each other with respect to the extracted model parameters. This is because, in principle, an LTI circuit can always be represented by its Norton or Thevenin equivalent, regardless of the external configuration.

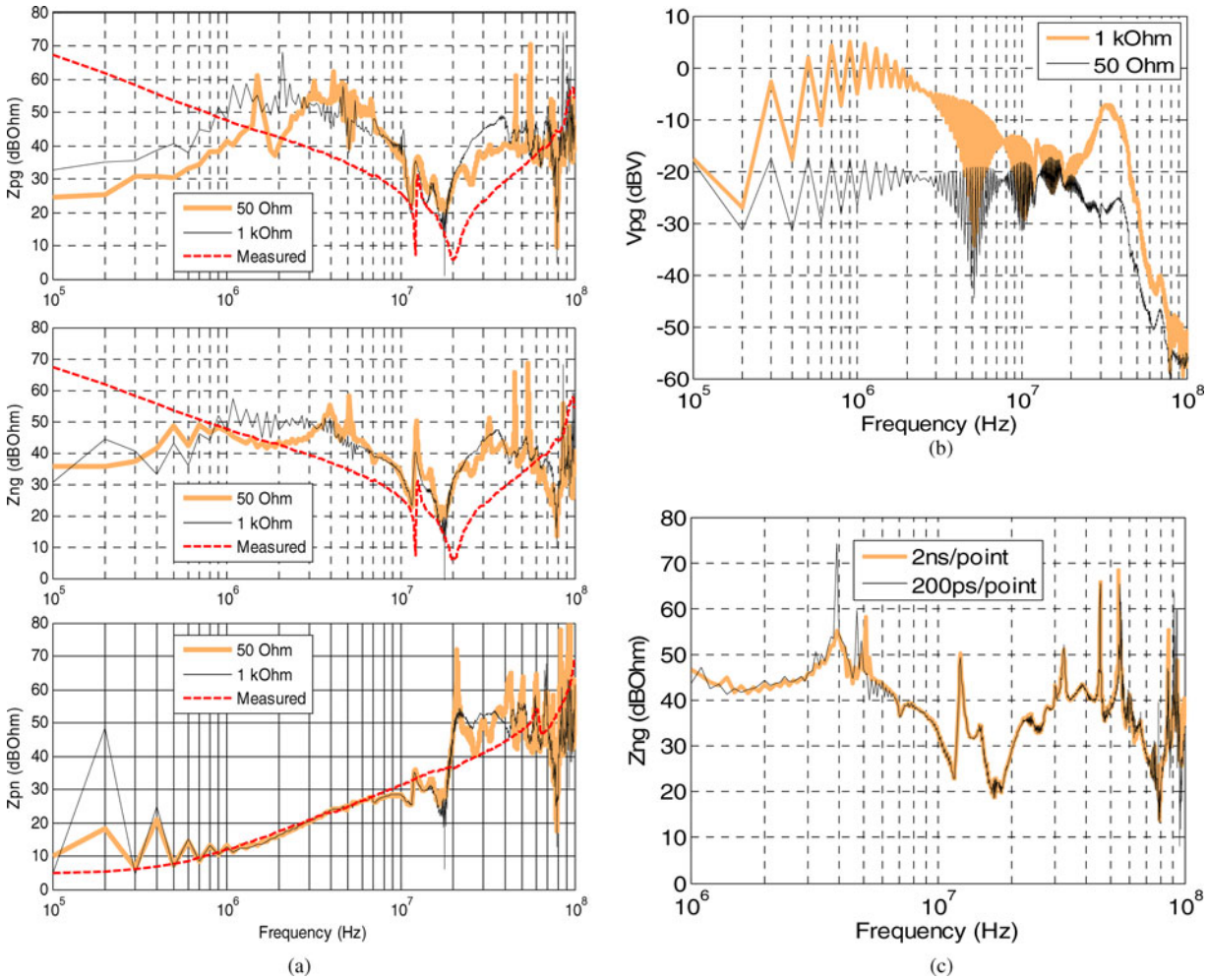


Fig. 10. (a) Extracted impedances $Z_{\rm PG}$, $Z_{\rm NG}$, and $Z_{\rm PN}$ of the three-terminal model. (b) Comparison of measured voltage on 1 kΩ LISN and 50 Ω LISN for the nominal case. (c) Effect of sampling frequency on extracted model impedances from the 50 Ω LISN.

Fig. 9 shows the comparison of $I_{\rm PG}$ and $I_{\rm NG}$ for the models created from the 50 Ω and 1 kΩ LISNs. It is clear that the extracted frequency-domain current sources do not show any significant difference when extracted from 50 Ω or 1 kΩ at most frequencies.

Fig. 10(a) shows the comparison of extracted model impedances $Z_{\rm PG}$, $Z_{\rm NG}$, and $Z_{\rm PN}$. $Z_{\rm PN}$ is almost the same for both models as this impedance is dominated by the inductance of the input bus and the 47 $\mu$F input capacitors between P and N terminals. From $Z_{\rm PG}$ and $Z_{\rm NG}$, the CM capacitive coupling path is evident. Capacitive behavior can be seen in frequency range from 1 to 10 MHz. Above 10 MHz, several spikes can be seen in the identified model impedances. However, due to better signal-to-noise (S/N) ratio, the spikes in the impedances extracted from 1 kΩ LISN are much lesser. Fig. 10(b) shows the comparison of measured voltage on the positive side of 1 kΩ and 50 Ω LISNs for the nominal case. It can be seen that at most frequencies, the measured voltage in the case of 1 kΩ LISN is about 10 dB higher than that of the 50 Ω LISN indicating better S/N ratio. The smaller amplitude, especially at higher frequencies, may also cause numerical ill-conditioning of the system of equations. To show this effect, the data measured on 50 Ω LISN was resampled at 2-ns/point resolution and the model impedances were extracted like before. Fig. 10(c) shows the comparison of identified $Z_{\rm NG}$ from the original dataset (200 ps/point) and the resampled one. At around 5 MHz and at higher frequencies, where the amplitude of the measured voltage was low [see Fig. 10(b)], some new spikes can be observed now. The 1 kΩ LISN was, however, found to be immune to changes in sampling frequency. Thus, the 1 kΩ LISN is suited better for extraction of model parameters as it provides better S/N ratio.

Fig. 10(a) also shows direct measurements of input impedances. These measurements were performed using an impedance analyzer (Agilent 4294A) when the converter was under zero dc bias (converter was switched OFF) condition. The DM impedance $Z_{\rm PN}$ was measured between terminals P and N with the converter isolated from the ground. Direct measurements of $Z_{\rm PG}$ and $Z_{\rm NG}$ were obtained by assuming them to be equal to one-half of the measured CM impedance between P-N short circuited and the ground. It can be observed that the

extracted CM impedances ($Z_{\rm PG}$ and $Z_{\rm NG}$) are asymmetric in the capacitive region. The real topological variation of the CM impedances, which may be different due to the geometry of the converter, can be observed here. The CM impedances are also quite different from the ones obtained by direct measurements. The reason for this difference is that under zero dc bias conditions, the IGBT's impedance is much smaller than the CM impedances. The IGBT output capacitance under zero bias is very large (nanofarad range) compared to parasitic capacitance between the converter and the heat sink (picafarad range). Thus, all parasitic CM capacitances to heat sink appear in parallel. This is evident from Fig. 10(a) as the measured CM capacitance is larger than the ones extracted by the terminal modeling approach. The extracted DM impedance, on the other hand, was a good match with the measured DM impedance except at high frequencies. Thus, the terminal modeling technique is useful in estimating model impedances in real operating conditions. Unlike the extracted model impedances, the measurements from impedance analyzer do not show any spikes. Moreover, above 10 MHz, there is a mismatch between the extracted $Z_{\rm PN}$ and the measured $Z_{\rm PN}$ from the impedance analyzer. This is because the impedance analyzer uses an internal sweep-frequency source that keeps constant and adequately large amplitude over the entire frequency range, thus producing good S/N ratio at all frequencies. The terminal modeling procedure, on the other hand, uses the switching noise from the converter to extract model impedances indirectly. The amplitude of this noise drops at higher frequency as seen in Fig. 10(b), leading to degradation in S/N ratio and error in estimation of impedances.

## V. Model Errors

### A. Effect of LISN Impedance

The extracted CM impedances ($Z_{\rm PG}$ and $Z_{\rm NG}$) seem to be inductive below 1 MHz. This is unrealistic because at lower frequencies, CM impedance must be capacitive. It was shown earlier [22] and [23] that in order to correctly identify the model impedances, the LISN impedance must be within an order of magnitude of the unknown impedance. To get an intuitional understanding of the mathematical derivation in [22] and [23], let us consider the example shown in Fig. 11. Here, an arbitrary two-terminal Norton equivalent network is attached to the LISN. It can be seen that if all measurements are performed across 1 kΩ resistor, then the inductor of the LISN is in parallel with $Z_N$. If $Z_N$ is a small capacitor (100–300 pF), then at lower frequencies, the impedance of the LISN inductor is much smaller than $Z_N$. Thus, voltage measurements at lower frequencies are dominated by the LISN inductor and identification of $Z_N$ becomes difficult. On the other hand, the DM impedance $Z_{\rm PN}$ of Fig. 7 can be correctly identified with this LISN as it is well below the LISN impedances at lower frequencies.

The aforementioned problem can be avoided by using a series insertion method as reported in [18] or by estimating the low-frequency CM impedance assuming capacitive behavior and extrapolating its value from the higher frequency measurements. Since all experiments shown here use the same LISN, no such corrections were found necessary.

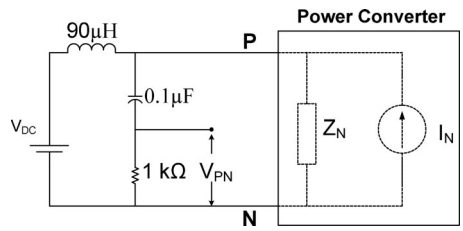


Fig. 11. Two-terminal network connected to a LISN.

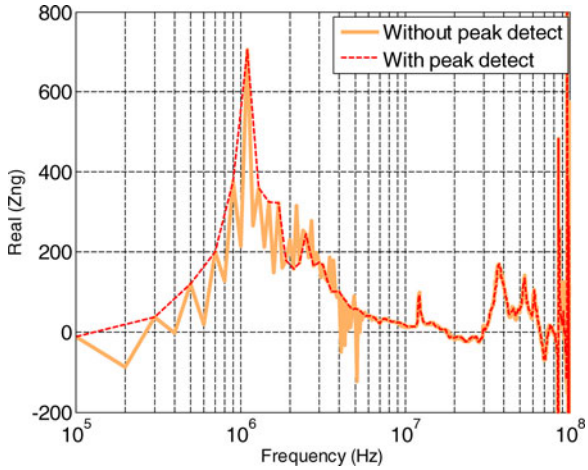


Fig. 12. Real parts of extracted CM impedance $Z_{\rm NG}$.

### B. Identifying Real Parts of Model Impedances

An issue that has never been reported before is that the terminal modeling technique can result in impedances $Z_{\rm PG}$, $Z_{\rm NG}$, and $Z_{\rm PN}$ that have negative real parts at certain frequencies. As an example, the real parts of $Z_{\rm NG}$ are plotted in Fig. 12. The negative real parts do not have any physical significance. Two reasons were identified for this kind of model error.

The first reason is that the amplitude of measured voltages at certain frequencies may be very small, and hence, the system of equations can get numerically ill-conditioned at those frequency points. A simple peak detect algorithm was used to eliminate them. Frequency points where the amplitude of the measured voltages was found to be smaller than the adjacent frequency points were removed. The model was then extracted using the modified frequency-domain data, and the real parts of the resulting $Z_{\rm NG}$ are plotted in Fig. 12 as well. It can be seen that at frequencies (e.g., 200 kHz), where the measured voltage was found to be low, the real part became negative, but with peak detection this frequency point was eliminated. In Figs. 9 and 10(a), a spike at 200 kHz can be observed for the same reason.

The second reason is that the real part of the impedance may be very small compared to its imaginary part. In Fig. 10(a), spike at around 1 MHz can be observed. This occurs at the parallel resonance between the CM capacitor and the LISN inductor [see $Z_{\rm PG}$ and $Z_{\rm NG}$ in Fig. 10(a)]. The real part here should approach 1 kΩ (LISN resistance). It can be seen from Fig. 12 that the identification of the real part starts to improve as they become significantly large in comparison to the imaginary part. However, even after peak detection some frequency points (e.g.,

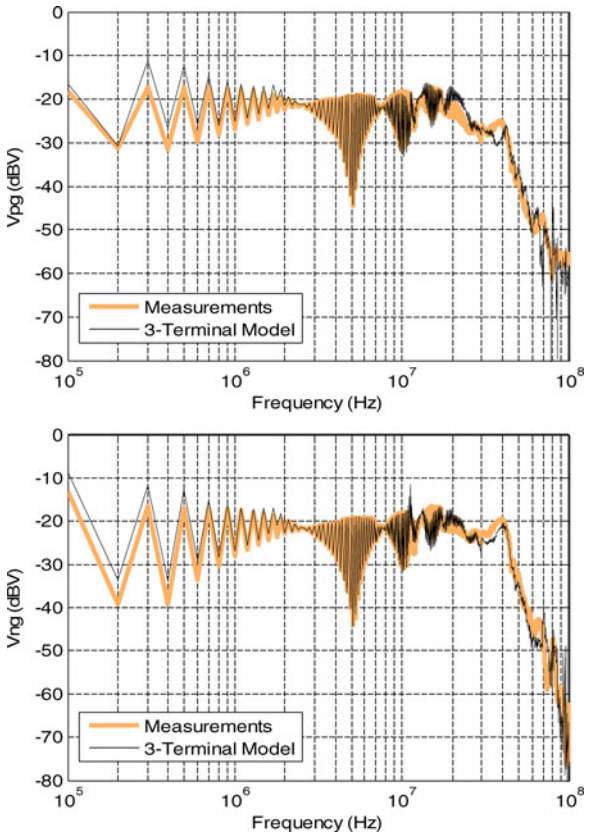


Fig. 13. Comparison of the measured and predicted conducted emissions at the positive and the negative terminal ($V_{\mathrm{PG}}$ and $V_{\mathrm{NG}}$) of 50 Ω LISN by a model created from 1 kΩ LISN.

at 100 kHz and around 20–30 MHz) are still negative because the real part here is very small compared to the imaginary part. At these frequencies, the real part of the impedances can be set to positive or to zero without loss of accuracy as their contribution is anyway negligible.

## VI. Model Validation

Two modes were created as mentioned before, one with a 1 kΩ LISN and the other with a 50 kΩ LISN. First, the model created from the 1 kΩ LISN was used to predict conducted emissions for the 50 Ω LISN. Fig. 13 shows the comparison of predicted conducted emissions with the actual measurements of conducted emissions on a 50 Ω LISN. The predictions made by the three-terminal model match well with the measurements from 100 kHz, which is the switching frequency of the buck converter, up to 100 MHz at almost all frequencies. The error is less than 6 dB up to 70 MHz. These predictions are computed in a math tool and show results for all frequency points including the ones that have a negative real part of model impedances.

Fig. 14 again gives the prediction results (only for the positive side of the LISN) by a model created with a 1 kΩ LISN for a 50 Ω LISN. This time, however, all the negative real parts of the model impedances were set to positive. As explained earlier, if the real part of the impedance is not significant compared to its imaginary part, this manipulation should not affect the EMI

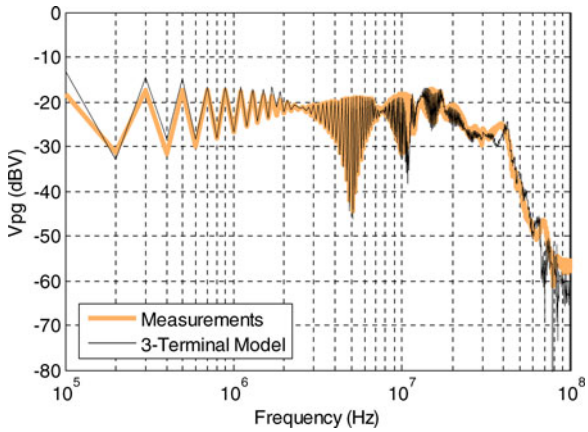


Fig. 14. Comparison of the measured and predicted conducted emissions at the positive terminal $V_{\mathrm{PG}}$ of 50 Ω LISN by a model created from 1 kΩ LISN with all negative real parts of model impedances manually changed to positive.

prediction results. Compared to prediction of $V_{\mathrm{PG}}$ in Fig. 14, no significant difference is observed in prediction accuracy. In fact, with the impedances now having a physical meaning, the model can now be made to run on circuit simulation software. Lumped circuit equivalent models of any external networks like cables, EMI filters, etc., can now be simulated with the terminal model of the converter to evaluate their effects on conducted emissions. The noise impedances can now be used for designing and optimizing EMI filters as well.

The model created with the 50 Ω LISN was then used to estimate conducted emissions for the 1 kΩ LISN. The results obtained were compared with measured conducted emissions values on the 1 kΩ LISN in Fig. 15. Again prediction for only the positive side of the LISN is shown here. Negative side results were found to be similar. It can be seen that the model created from the 50 Ω LISN failed to predict conducted emissions at both low and high frequencies. The reason for poor prediction at higher frequencies can be due to a lower impedance of the 50 Ω LISN compared to the DM impedance of the system. This error is similar to the one explained in Section V. The S/N ratio of measured voltages on a 50 Ω LISN is also worse compared to voltages measured on a 1 kΩ LISN [see Fig. 10(b)]. At lower frequencies as well, the predictions are not good enough. Thus, even though in principle there should not be any difference between models extracted from 50 Ω and 1 kΩ LISNs, due to measurement related errors, one of them may be more accurate than the other.

## VII. Three-Terminal Modeling of DC–AC Systems

In [26], a three-terminal model was used to model a half-bridge inverter. The results were good up to at least 30 MHz. The extension of this technique to dc–ac systems was shown to be fairly easy. Since ac systems have a variable operating point over the line cycle, the conducted emissions also change and repeat with line frequency. Thus, in order to capture the temporal variation in EMI, the noise signature over the entire line cycle is required. This can lead to very large datasets. Some techniques have been discussed in [38] to reduce the size

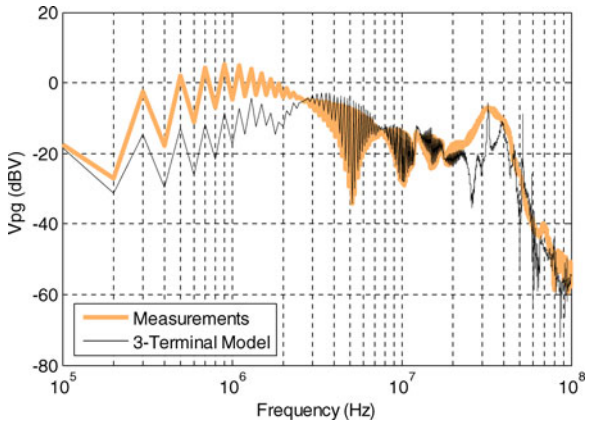


Fig. 15. Comparison of the measured and predicted conducted emissions at the positive terminal $V_{PG}$ of 1 kΩ LISN by a model created from 50 Ω LISN.

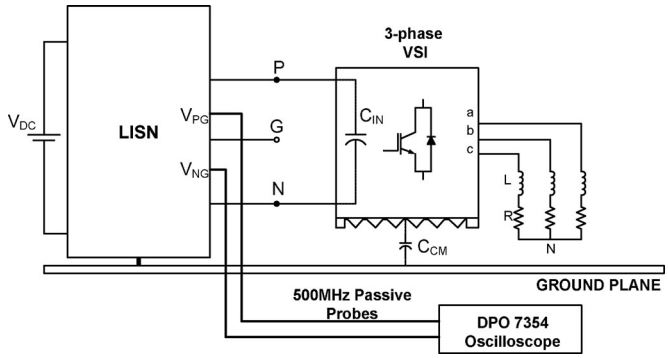


Fig. 16. Experimental setup for extraction of the three-terminal model of a three-phase VSI.

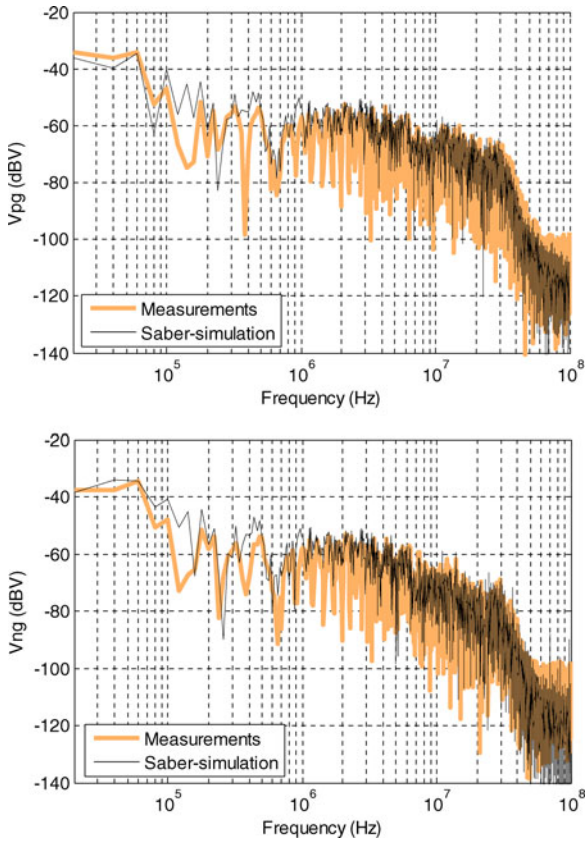


Fig. 17. Comparison of measured and predicted conducted emissions at the positive and the negative terminal ($V_{PG}$ and $V_{NG}$) of 50 Ω LISN by a model created from 1 kΩ LISN for three-phase VSI.

of the datasets without significantly sacrificing accuracy. The terminal modeling technique is now applied to a three-phase voltage source inverter (VSI).

Fig. 16 shows the test setup used. The three-phase inverter used here has an IGBT module (Fuji 6MBP30RH060-50) and a resistive–inductive (*RL*) load of 15 Ω and 600 $\mu$H, respectively. A decoupling capacitor (film type) of 0.22 $\mu$F and a bulk capacitor (electrolytic) of 47 $\mu$F were placed at the input side of the VSI ($C_{IN}$). The switching frequency was set to 20 kHz and line frequency was 400 Hz. The converter was running at 1.2 kW. The LISN used was the same as shown in Fig. 6. A high bandwidth scope was used to record the waveforms for the entire line cycle with a time resolution of 5 ns/point. The model was extracted exactly as described in Section II.

The predictions were carried out using a circuit model in (SABER® simulator) this time. The model was implemented as a lookup table with the information of all impedance and current sources listed frequency point by point. Another way is to fit an *RLC* circuit in the model impedances [18] with the sources implemented in time domain. A model created from 1 kΩ LISN was then used to predict EMI on a 50 Ω LISN. Fig. 17 shows these results. Again, a good matching of predicted and measured results can be seen at most frequencies between 20 kHz and 100 MHz.

## VIII. Conclusion

This paper has presented the merits and challenges of EMI terminal modeling technique for switching power converters and extended the modeling technique to three-phase ac systems. It was shown that the presence of dominant input parasitics and an input capacitor helps in approximating the converter as a linear network when looked from the dc input side. The terminal modeling approach is gray box in nature as it requires an estimation of the order of the unknown model impedances; however, it was shown that such an estimation can be easily obtained by a direct measurement of these impedances. This paper also discussed the problems associated with identification of model impedances due to numerical errors and provides simple ways to correct them.

In all, the terminal modeling technique is promising as the models were shown to be accurate even outside the conducted emissions range. Moreover, being numerical the terminal model can easily run on a math tool enabling faster prediction results when compared to circuit simulations of physics-based models.

## Acknowledgment

The authors would like to acknowledge the consistent support provided by Nicolas Gazel and Regis Meuret from Hispano-Suiza, Safran Power.

## REFERENCES


[1] Y. Maillet, L. Rixin, W. Shuo, F. Wang, R. Burgos, and D. Boroyevich, "High-density EMI Filter design for DC-fed motor drives," in *Proc. 24th Annu. IEEE Appl. Power Electron. Conf. Expo*., 2009, pp. 1998–2005.

[2] S. D. Round, P. Karutz, M. L. Heldwein, and J. W. Kolar, "Towards a 30 kW/liter, three-phase unity power factor rectifier," in *Proc. Power Convers. Conf*., 2007, pp. 1251–1259.

[3] Z. Huibin, L. Jih-Sheng, A. R. Hefner, Jr., T. Yuqing, and C. Chingchi, "Analysis of conducted EMI emissions from PWM inverter based on empirical models and comparative experiments," in *Proc. IEEE Power Electron. Spec. Conf*., 1999, vol. 2, pp. 861–867.

[4] M. Moreau, N. Idir, and P. Le Moigne, "Modeling of conducted EMI in adjustable speed drives," *IEEE Trans. Electromagn. Compat*., vol. 51, no. 3, pp. 665–672, Aug. 2009.

[5] L. Ran, S. Gokani, J. Clare, K. J. Bradley, and C. Christopoulos, "Conducted electromagnetic emissions in induction motor drive systems—I. Time domain analysis and identification of dominant modes," *IEEE Trans. Power Electron*., vol. 13, no. 4, pp. 757–767, Jul. 1998.

[6] P. Xuejun, Z. Kai, K. Yong, and C. Jian, "Analytical estimation of common mode conducted EMI in PWM inverter," in *Proc. Conf. Rec. IEEE IAS Annu. Meeting*, 2004, vol. 4, pp. 2651–2656.

[7] F. Giezendanner, J. Biela, J. W. Kolar, and S. Zudrell-Koch, "EMI noise prediction for electronic ballasts," *IEEE Trans. Power Electron*., vol. 25, no. 8, pp. 2133–2141, Aug. 2010.

[8] B. Revol, J. Roudet, J. L. Schanen, and P. Loizelet, "EMI study of three-phase inverter-fed motor drives," *IEEE Trans. Ind. Appl*., vol. 47, no. 1, pp. 223–231, Jan./Feb. 2011.

[9] Y. Koyama, M. Tanaka, and H. Akagi, "Modeling and analysis for simulation of common-mode noises produced by an inverter-driven air conditioner," *IEEE Trans. Ind. Appl*., vol. 47, no. 5, pp. 2166–2174, Sep./Oct. 2011.

[10] L. M. Schneider, "Noise source equivalent circuit model of off-line converters and use in input filter design," in *Proc. IEEE EMC Symp*., 1983, pp. 167–175.

[11] L. Ran, J. C. Clare, K. J. Bradley, and C. Christopoulos, "Measurement of conducted electromagnetic emissions in PWM motor drive systems without the need for an LISN," *IEEE Trans. Electromagn. Compat*., vol. 41, no. 1, pp. 50–55, Feb. 1999.

[12] J. Meng, W. Ma, and L. Zhang, "Determination of noise source and impedance for conducted EMI prediction of power converters by lumped circuit models," in *Proc. IEEE Power Electron. Spec. Conf*., 2004, vol. 4, pp. 3028–3033.

[13] H. Rebholz and S. Tenbohlen, "Prospects and limits of common- and differential-mode separation for the filter development process," in *Proc. EMC Europe Int. Symp*., 2008, pp. 1–6.

[14] Z. Dongbing, C. Dan, and D. Sable, "Non-intrinsic differential mode noise caused by ground current in an off-line power supply," in *Proc. IEEE Power Electron. Spec. Conf*., 1998, vol. 2, pp. 1131–1133.

[15] J. Meng and W. Ma, "A new technique for modeling and analysis of mixed-mode conducted EMI noise," *IEEE Trans. Power Electron*., vol. 19, no. 6, pp. 1679–1687, Nov. 2004.

[16] A. Perez, A. M. Sanchez, J. R. Regue, M. Ribo, P. Rodriguez-Cepeda, and F. J. Pajares, "Characterization of power-line filters and electronic equipment for prediction of conducted emissions," *IEEE Trans. Electromagn. Compat*., vol. 50, no. 3, pp. 577–585, Aug. 2008.

[17] H. M. Rebholz, S. Tenbohlen, and W. Kohler, "Time-domain characterization of RF sources for the design of noise suppression filters," *IEEE Trans. Electromagn. Compat*., vol. 51, no. 4, pp. 945–952, Nov. 2009.

[18] M. Jin, M. Weiming, P. Qijun, Z. Zhihua, and Z. Lei, "Noise source lumped circuit modeling and identification for power converters," *IEEE Trans. Ind. Electron*., vol. 53, no. 6, pp. 1853–1861, Dec. 2006.

[19] L. Qian, W. Fei, and D. Boroyevich, "Modular-terminal-behavioral (MTB) model for characterizing switching module conducted EMI generation in converter systems," *IEEE Trans. Power Electron*., vol. 21, no. 6, pp. 1804–1814, Nov. 2006.

[20] L. Qian, F. Wang, and D. Boroyevich, "Conducted-EMI prediction for AC converter systems using an equivalent modularterminal behavioral (MTB) source model," *IEEE Trans. Ind. Appl*., vol. 43, no. 5, pp. 1360–1370, Sep./Oct. 2007.

[21] M. Hosoya, "The simplest equivalent circuit of a multi-terminal network," Bulletin College Sci.—Univ. Ryukyus, pp. 1–10, 2000.

[22] A. C. Baisden, D. Boroyevich, and W. Fei, "Generalized terminal modeling of electromagnetic interference," *IEEE Trans. Ind. Appl*., vol. 46, no. 5, pp. 2068–2079, Sep./Oct. 2010.

[23] A. C. Baisden, D. Boroyevich, and F. Wang, "EMI Terminal Modeling," in *Conf. Rec. IEEE IAS Annu. Meeting*, 2008, pp. 1–8.

[24] M. Foissac, J. L. Schanen, and C. Vollaire, "'Black box' EMC model for power electronics converter," in *Proc. IEEE Energy Convers. Congr. Expo*., 2009, pp. 3609–3615.

[25] H. Bishnoi, A. C. Baisden, P. Mattavelli, and D. Boroyevich, "EMI modeling of buck converter using a generalized terminal model," in *Proc. Conf. Grand Challenges Modeling Simulation*, 2010, pp. 158–164.

[26] H. Bishnoi, A. C. Baisden, P. Mattavelli, and D. Boroyevich, "EMI modeling of half-bridge inverter using a generalized terminal model," in *Proc. IEEE Appl. Power Electron. Conf. Expo*., Mar. 2011, pp. 468–474.

[27] X. Lei, F. Feng, and S. Jian, "Behavioral modeling methods for motor drive system EMI design optimization," in *Proc. IEEE Energy Convers. Congr. Expo*., 2010, pp. 947–954.

[28] Q. Tao, J. Graham, and S. Jian, "Characterization of IGBT modules for system EMI simulation," in *IEEE Appl. Power Electron. Conf. Expo*., Feb. 2010, pp. 2220–2225.

[29] C. Jettanasen, F. Costa, and C. Vollaire, "Common-mode emissions measurements and simulation in variable-speed drive systems," *IEEE Trans. Power Electron*., vol. 24, no. 11, pp. 2456–2464, Nov. 2009.

[30] D. Labrousse, B. Revol, and F. Costa, "Common-mode modeling of the association of N-switching cells: Application to an electric-vehicle-drive system," *IEEE Trans. Power Electron*., vol. 25, no. 11, pp. 2852–2859, Nov. 2010.

[31] Z. Dongbing, D. Y. Chen, M. J. Nave, and D. Sable, "Measurement of noise source impedance of off-line converters," *IEEE Trans. Power Electron*., vol. 15, no. 5, pp. 820–825, Sep. 2000.

[32] K. Kiatgamjorn, P. Boonma, and W. Khan-ngern, "The study of input impedance of switched mode power supply," in *Proc. Int. Conf. Electr. Eng./Electron. Comput. Telecommun. Inf. Technol*., 2008, pp. 1049–1052.

[33] S. Kye Yak and D. Junhong, "Measurement of noise source impedance of SMPS using a two probes approach," *IEEE Trans. Power Electron*., vol. 19, no. 3, pp. 862–868, May 2004.

[34] V. Tarateeraseth, H. Bo, S. Kye Yak, and F. G. Canavero, "Accurate extraction of noise source impedance of an SMPS under operating conditions," *IEEE Trans. Power Electron*., vol. 25, no. 1, pp. 111–117, Jan. 2010.

[35] W. Yan, Y. Zhao, X.-Q. Lu, Y.-h. Dong, and W. Feng, "A modified EMI noise source impedance modeling by employing two resistances calibration and Levenberg-Marquardt's method," in *Proc. Int. Conf. Microw. Millimeter Wave Technol*., 2010, pp. 2021–2024.

[36] B. Zhao, M. Zhao, Z. Feng, L. Shui, and M. Yao, "An improved dual-probe approach to measure noise source impedance," in *Proc. Asia-Pacific Symp. Electromagn. Compat*., 2010, pp. 214–217.

[37] V. Tarateeraseth, S. Kye Yak, F. G. Canavero, and R. W. Chang, "Systematic electromagnetic interference filter design based on information from in-circuit impedance measurements," *IEEE Trans. Electromagn. Compat*., vol. 52, no. 3, pp. 588–598, Aug. 2010.

[38] A. C. Baisden, "Generalized terminal modeling of electro-magnetic interference," Ph.D. dissertation, Dept. Elect. Eng., Virginia Tech, Blacksburg, 2010.


**Hemant Bishnoi** (S'10) received the B.S. degree in electronics and telecommunication engineering from the University of Mumbai, Mumbai, India, in 2007, and the M.S. degree in electrical engineering from the Electromagnetic Compatibility Laboratory, University of Missouri-Rolla, Rolla, in 2009. He is currently working toward the Ph.D. degree in electrical engineering from the Centre for Power Electronics Systems, Virginia Tech., Blacksburg.

In the summer of 2010, he has worked as a Signal Integrity Analysis Engineer at Johnson Controls, Holland, MI, and in 2011, as an intern at Hispano-Suiza, Safran Power, France. His research interests include electromagnetic modeling and simulation, signal/power integrity, and electromagnetic compatibility.

**Andrew Carson Baisden** (S'03–M'09) received the B.S. degree in electrical engineering from the Illinois Institute of Technology, Chicago, in 2003, the B.S. degree in mathematics from Benedictine University, Lisle, IL, in 2003, and the M.S. and Ph.D. degrees in electrical engineering from the Center for Power Electronics Systems (CPES), Virginia Tech, Blacksburg, in 2006 and 2009, respectively.

He was a Research Lab Assistant at Argonne National Laboratories in 2000–2002. In the summer of 2006, he was a Power Electronics Development Engineer for Rockwell Automation. From 2003 to 2009, he was with CPES as a Graduate Research Assistant. He then joined the Johns Hopkins University Applied Physics Laboratory, Laurel, MD, as a Power Electronics Engineer for space applications. His research interests include power conversion systems and analog design, electromagnetic interference/electromagnetic compatibility, electronics packaging, and integrated power electronic systems.

**Paolo Mattavelli** (S'95–A'96–M'00–SM'10) received the M.S. (Hons.) and Ph.D. degrees in electrical engineering from the University of Padova, Padua, Italy, in 1992 and 1995, respectively.

From 1995 to 2001, he was a Researcher at the University of Padova. From 2001 to 2005, he was an Associate Professor at the University of Udine, where he led the Power Electronics Laboratory. In 2005, he joined the University of Padova in Vicenza with the same duties. In 2010, he joined Virginia Tech, Blacksburg, as a Professor, where he is also a member of the Center for Power Electronics Systems. His major field of interest includes analysis, modeling and control of power converters, digital control techniques for power electronic circuits and grid-connected converters for power quality, and renewable energy systems. In these research fields, he has been leading several industrial and government projects.

Dr. Mattavelli has served as an Associate Editor for the IEEE TRANSACTIONS ON POWER ELECTRONICS since 2003. From 2005 to 2010, he was the IPCC (Industrial Power Converter Committee) technical review chair for the IEEE TRANSACTIONS ON INDUSTRY APPLICATIONS. For terms 2003–2006 and 2006–2009, he was also a member-at-large of the IEEE Power Electronics Society's Administrative Committee. He also received in 2005 and 2006 the Prize Paper Award in the IEEE Transactions on Power Electronics, and in 2007, a second place in the Prize Paper Award at the IEEE Industry Application Annual Meeting.

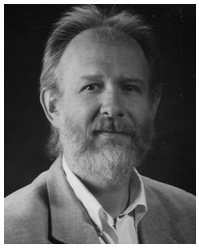

**Dushan Boroyevich** (S'81–M'86–SM'03–F'06) received the Dipl.Ing. degree from the University of Belgrade, Belgrade, Serbia, in 1976, the M.S. degree from the University of Novi Sad, Novi Sad, Serbia, in 1982, and the Ph.D. degree from Virginia Tech, Blacksburg, in 1986.

From 1986 to 1990, he was an Assistant Professor and Director of the Power and Industrial Electronics Research Program in the Institute for Power and Electronic Engineering, University of Novi Sad, and later, Acting Head of the Institute. He then joined the Bradley Department of Electrical and Computer Engineering, Virginia Tech as an Associate Professor. He is currently the American Electric Power Professor in the department and the Co-Director of the Center for Power Electronics Systems, Virginia Tech. His research interests include multiphase power conversion, electronic power distribution systems, power electronics systems modeling and control, and multidisciplinary design optimization.

Dr. Boroyevich is a recipient of the IEEE William E. Newell Power Electronics Technical Field Award. He is the President of the IEEE Power Electronics Society for 2011–2012.